JACS
JOURNAL OF THE AMERICAN CHEMICAL SOCIETY
pubs.acs.org/JACS
Communication

Electrochemical Control over Electron Density of InAs Quantum Dots

Yan B. Vogel,* Rui Tao,# Hua Chen,# Lorenzo J.A. Ferraresi, Simon C. Boehme, Dmitry N. Dirin, Ivan Shorubalko, Arjan J. Houtepen, and Maksym V. Kovalenko*

Cite This: J. Am. Chem. Soc. 2026, 148, 3938−3943
Read Online
ACCESS | Metrics & More | Article Recommendations | Supporting Information

ABSTRACT: Control over the electron density and conductivity is a cornerstone of semiconductor technology. Here, we report electrochemical control over electron density and conductivity in films of InAs colloidal quantum dots (QDs) capped with ethanedithiol ligands. The quantum-confined twofold degenerate $1S_{1/2}(e)$ electron state can be reversibly and completely filled. Increasing the electron population yields four bleach features in the optical-absorption spectrum associated transitions to the $1S_{1/2}(e)$ state, and state-resolved electronic conductivity which follows the $1S_{1/2}(e)$ density of states, reaching a maximum of 0.45 S/m at 0.5 electrons per QD. The absence of 1P(e) bleach features and state-resolved conductivity imply a wide separation between the $1S_{1/2}(e)$ and 1P(e) states resulting in electronic transport between 1S(e) states exclusively. The reversible electrochemistry of InAs QDs films allows determination of the absolute energy levels. InAs QDs of 4.2 nm in edge length and capped with ethanedithiol ligands are natively n-doped with the Fermi level at −4.6 eV, the $1S_{1/2}(e)$ state at −4.28 eV and the $1S_{3/2}(h)$ state at −5.54 eV vs vacuum. This work establishes a way to precisely control the charge carrier density and conductivity and gives insights into the charge transport properties and electronic structure of InAs QD films, opening the possibility of making devices with InAs QDs in which the charge carrier density is precisely controlled electrochemically.

Increasing automation, self-driving cars, smart appliances, healthcare devices and security systems require the development of more efficient, cheaper, and environmentally friendly infrared photodetectors[1] and light-emitting devices.[2] Colloidal quantum dots (QDs) meet these criteria because of their cheap solution processability and excellent and tunable optoelectronic properties.[3] Devices based on Pb[4−6] and Cd[7−9] chalcogenide QDs have shown remarkable performance.[10] However, their use is restricted by the Restriction of Hazardous Substances Directive (RHoS).[11] In this regard, InAs QDs offer a great opportunity as an RHoS-compliant material.[12,13]

Crucial for the adoption of InAs QDs (and other QDs) in future semiconductor technologies is controlling charge carrier density, i.e. doping.[14−19] However, doping InAs QDs remains challenging.[12] Some works have reported the incorporation of metals, but this usually results in only mild doping and has detrimental effects on the electronic and structural properties of the QDs.[12,17,20−23] Electrochemical doping offers a more controllable and higher extent of doping.[24−27] Electrochemical doping has been demonstrated for several QD materials, including ZnO,[28−33] Pb(S, Se),[34−37] Cd(Se, Te),[38−45] Hg(S, Se, Te),[46−48] $CsPbBr_3$,[49] Si[50] and $CuInS_2$.[51,52] Here we accomplish electrochemical charge carrier modulation in InAs QDs. We use *in situ* visible and near-infrared absorption spectroscopy during electrochemical doping to quantify the charge-carrier density,[53] and electrochemical transistor measurements[54] to determine the electron conductivity and electron mobility in InAs QD films with different doping densities.

We synthesized InAs QDs following Song et al.,[55−57] with tris(trimethylsilyl)arsine and indium oleate precursors (Supporting Information (SI), section S1). This results in tetrahedral oleate terminated InAs QDs of 4.2 nm in edge length (Figure S6) with a band edge absorption at 926 nm (Figure 1, red dashed line). We prepared InAs QD films by spin coating the oleate terminated QDs onto indium−tin-oxide (ITO) coated glass substrates followed by a layer-by-layer solid-state ligand exchange with ethanedithiol (EDT) ligands (Figure S7) to enhance carrier transport across the film.[58,59] The band-edge absorption of the InAs QD film with EDT

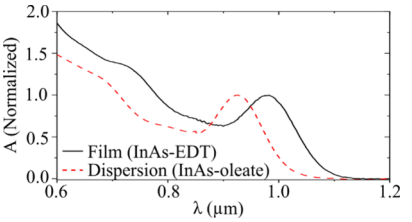

Figure 1. Absorbance (A) spectra of InAs QDs of 4.2 nm in edge length in an octane dispersion with oleate ligands (red dashed line) and as a film with ethanedithiol ligands (black solid line).

Received: November 26, 2025
Revised: January 15, 2026
Accepted: January 16, 2026
Published: January 22, 2026

https://doi.org/10.1021/jacs.5c21128
J. Am. Chem. Soc. 2026, 148, 3938−3943

ligands (InAs-EDT) red shifts to 980 nm (Figure 1, black solid line). Subsequently, we measured the changes in the absorption spectrum of InAs-EDT while applying a potential via cyclic voltammetry (CV) in an electrolyte of 0.1 M $LiClO_4$ in propylene carbonate under strictly anhydrous and anaerobic conditions (setup details in SI, section S2).

The CV of InAs-EDT shown in Figure 2A starts at the open-circuit potential (OCP), which is at −0.2 V (all potentials are

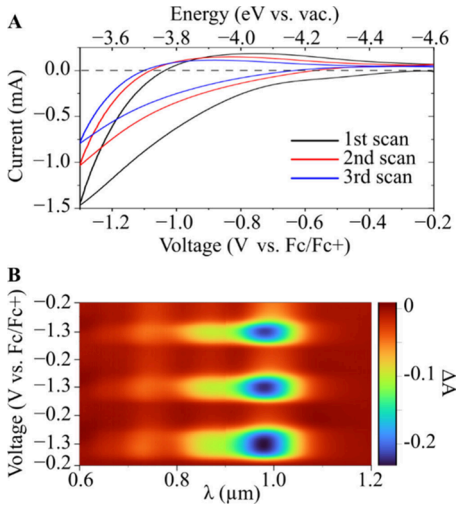

Figure 2. Reversible electron injection into InAs QDs. A) Cyclic voltammetry (CV, solid lines) at a scan rate of 100 mV/s and B) differential absorbance (ΔA) during the CV of the InAs-EDT QD film showing reversible bleaching of several optical transitions. The dashed line in A) is a blank measurement with a bare ITO electrode (Figure S9).

reported against the ferrocene/ferrocenium couple), and goes to −1.3 V and back to the OCP at a scan rate of 100 mV/s. The potential scan is repeated two more times. The data reported in Figure 2 and thereafter lie within the stable electrochemical window (between +0.45 and −1.3 V), defined as the potential region with reversible optical changes (see SI, Section S5). The CV shows an anodic-to-cathodic charge ratio (Q_a/Q_c) of 25% for the first scan. We attribute the relatively low Q_a/Q_c to the presence of redox active impurities, as previously reported.[25,60] Q_a/Q_c is expected to increase with (1) decreasing the cathodic vertex, (2) increasing the scan number and (3) increasing the scan rate.[35] Figure S8 shows that Q_a/Q_c increases to 35% for the second scan, to 55% for a cathodic vertex of −1.0 V, and to 95% at 500 mV/s. The differential absorbance (ΔA) spectra during the three CV scans show a reversible decrease in the absorbance (bleach) of several excitonic transitions (Figure 2B). The reversible bleach is evidence of electron injection into the 1Se level as it results from blocking of 1S transitions involving the 1Se level.[35,61]

Figure 3A shows the ΔA spectra as a function of potential (black solid lines, bottom) featuring bleach features at 980, 855, 731, and 652 nm, referred hereafter as transitions 1−4, respectively. The ΔA spectra can be described well (black dashed line, bottom) with a sum of four Gaussian transitions (red, blue, green, and pink dashed lines, respectively), exemplarily shown for the ΔA spectra at −1.3 V, i.e., at the most negative potential. To interpret the spectroelectrochemical data, we associate the observed spectral changes upon electron injection with the absorbance spectrum at OCP

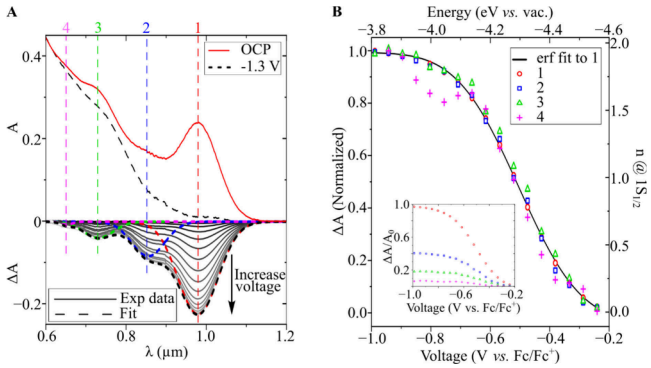

Figure 3. Reversible spectroscopic changes upon electron injection into InAs QDs. A) Absorbance (A) spectrum at OCP (red solid line, top) and −1.3 V (black dashed line, top), differential absorbance (ΔA) spectrum from OCP to −1.3 V (black solid lines, bottom) and Gaussian fits to the spectrum at −1.3 V (dashed lines, bottom) of InAs-EDT films. The vertical dashed lines indicate the peak wavelength of each Gaussian fit, labeled as transitions 1−4. B) Normalized ΔA at the peak position for transitions 1−4, respective $\Delta A/A_0$ (inset) and number of electrons per QD (n) at the $1S_{1/2}(e)$ level as a function of potential. The solid line is an error-function fit to the experimental data for transition 1.

(Figure 3A; red solid line, top) and with the reported transitions calculated from multiband effective mass theory.[62,63] Following Banin et al.,[62,63] we assign transition 1 to $1S_{3/2}(h)\rightarrow 1S_{1/2}(e)$. The bleached transitions 2−4 can be due to either electron filling of the $1S_{1/2}(e)$ level or electron filling of higher levels in the conduction band such as $1P_{3/2}(e)$. Transitions to the $1S_{1/2}(e)$ state would all bleach at the same potential, while transitions to the $1P_{3/2}(e)$ state would bleach at more negative potentials because the $1P_{3/2}(e)$ state lies higher in energy than the $1S_{1/2}(e)$ state. Figure 3B shows that transitions 1−4 all have the same potential dependence, and therefore, all correspond to transitions from an S(h) to the $1S_{1/2}(e)$ state. Therefore, we assign transitions 2−4 to $2S_{3/2}(h)\rightarrow 1S_{1/2}(e)$, $1S_{1/2}(h)\rightarrow 1S_{1/2}(e)$ and $2S_{1/2}(h)\rightarrow 1S_{1/2}(e)$, respectively.

Figure 3B also shows the dependence with potential of the number of electrons per QD (n) populating the $1S_{1/2}(e)$ state (red circles for the data and a line for the Gaussian fit). We extract n from the fractional bleach of the $1S_{3/2}(h)\rightarrow 1S_{1/2}(e)$ transition via $n(V) = g\Delta A(V)/A_0$, where g is the degeneracy of the $1S_{1/2}(e)$ level (g = 2 for InAs QDs). We observe that n increases until leveling off at n = 1.95, close to the theoretical value of n = 2.

Figure 4 shows the determined electronic structure, absolute energy levels of the involved states, and density of states (DOS) of the $1S_{1/2}(e)$ level (red circles for experimental data and black line for the Gaussian fit), obtained from the derivative of n with respect to the potential ($-dn/dV$). The maximum of this Gaussian is the $1S_{1/2}(e)$ energy level, which is at −4.28 eV. The $1S_{3/2}(h)$ level is obtained by adding the optical bandgap energy (1.17 eV) to this value, placing it at −5.54 eV (assuming a negligible exciton binding energy). Similarly, this allows us to infer the absolute energy level of the rest of the involved transitions. Figure 4 also shows that the Fermi level (E_F, red dashed line), determined from the OCP, is 0.32 eV below $1S_{1/2}(e)$, indicating that these films are natively n-doped, in agreement with literature.[56] The blue bar in Figure 4 shows the ranges of doping levels reached in this work.

https://doi.org/10.1021/jacs.5c21128
J. Am. Chem. Soc. 2026, 148, 3938−3943

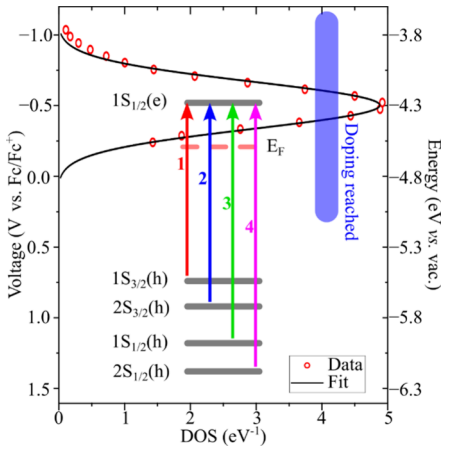

Figure 4. Electronic structure and absolute energy levels of InAs QDs of 4.2 nm in edge length. Band diagram, electronic transitions (vertical arrows), DOS of the $1S_{1/2}(e)$ level (red circles for data and black line for Gaussian fit), and doping level accomplished in this work (blue bar) for InAs QDs.

Even at the most negative potentials, where the $1S_{1/2}(e)$ level is completely filled, we do not observe any signs of the injection of 1P electrons. This implies that the separation between the 1P(e) and 1S(e) level is $\gg kT$, so thermal population of 1P(e) levels does not occur when the Fermi level is at 1S(e), and larger than the spread in energy due to size disorder. This has important consequences for electron transport in InAs films at different electron densities. Therefore, we performed electrochemical transistor measurements[24,26,28,34,37,46,47,49,53,54,64−69] on an InAs-EDT QD film with a band-edge absorption at 1065 nm (Figure S12), which allows the film conductivity and electron mobility to be measured as a function of potential or, equivalently, as a function of electron density, as discussed in detail in Section S6 of the SI. Figure 5A (black solid circles for data and dashed line

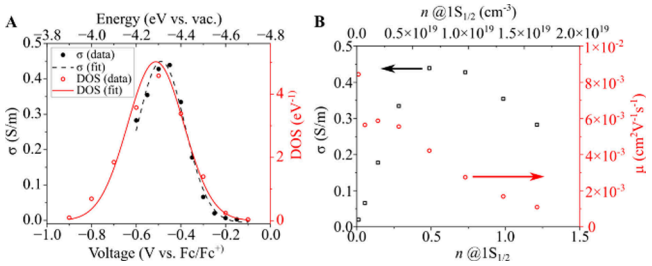

Figure 5. Electron conductivity and mobility of InAs QD films as a function of the charge carrier density. A) Plot of the conductivity (σ, black solid circles) superimposed to the DOS (red empty circles) as a function of potential. The lines are Gaussian fits to the experimental data. B) Plot of the electron conductivity (σ, black squares) and mobility (μ, red circles) as a function of the $1S_{1/2}(e)$ electron concentration (number of electrons per QD at the $1S_{1/2}$ level, n).

for a Gaussian fit) shows the conductivity at potentials from −0.15 V to −0.6 V. Figure 5A (red empty circles for data and solid line for a Gaussian fit) also shows the DOS of $1S_{1/2}(e)$ determined by spectroelectrochemistry (Figure S14). The conductivity closely follows the DOS, as theoretically predicted[70] but not frequently observed.[26,47] Within this potential range (from −0.15 V to −0.6 V) the changes in conductivity are completely reversible (Figure S15), confirming that the conductivity dependence is due to changes in the electron density. Decreasing the potential below −0.6 V leads to irreversible changes in conductivity (Figure S16), and therefore we report here conductivity and mobility values between OCP and −0.6 V.

Figure 5B shows the dependence of the electron conductivity (σ, black squares) and mobility (μ, red circles) of the InAs-EDT QD film on charge carrier density (n). σ first increases with n, reaches a maximum of 0.45 S/m around n = 0.5, and decreases for $n > 0.5$. μ shows a maximum of 9×10^{-3} $cm^2/V{\cdot}s$ at the lowest carrier density ($n = 0.005$) and decreases with increasing n. The electron mobility values are consistent with previously reported electron mobilities of 10^{-4}−10^{-2} $cm^2/V{\cdot}s$.[71−73]

A maximum conductance at partial filling of the 1S(e) levels and a decreasing mobility with increasing n are both consistent with state selective electron transport that takes place exclusively through the 1S(e) levels, combined with a narrow spread in 1S(e) site energies. In that limit the rate of electron transport, and hence the conductivity, scales as the product of the density donor states (i.e., $n_{1S_{(e)}} \approx n$) and the density as empty acceptor states (i.e., $2 - n_{1S_{(e)}}$), giving $\sigma \propto n(2 - n)$ and $\mu = \frac{\sigma}{en} \propto 2 - n$. The experimental data follow the general predicted features of a parabolic σ vs n relationship and an increase in μ with n. However, it also deviates in a few details: (1) the σ vs n relationship does not follow a symmetric parabola, with an increase in σ more pronounced than its decrease; (2) σ reaches a maximum at n = 0.5 instead of the theoretical n = 1; and (3) the decrease in mobility is not perfectly linear over the whole charge carrier density range. Nevertheless, the increase in μ with n and the parabolic σ vs n relationship are usually not observed because of energy disorder, resulting in activated transport that always grows with increasing Fermi level, and the contribution of higher energy levels (1P(e), 1D(e), . . .) to electron transport.[70] The observation of state selective transport is a testament to the narrow spread in 1S(e) energy levels and the large 1P(e) − 1S(e) energy separation. In other words, these InAs QDs are both highly monodisperse and show a very strong quantum confinement of the electrons.

In summary, InAs QDs show reversible and stable electrochemistry at potentials between +0.45 V and −1.30 V vs Fc/Fc^+. The reversible electrochemistry of InAs QDs opens the possibility for obtaining InAs QD devices where the charge carrier density is controlled electrochemically and the use of electrochemistry as a standard characterization technique for InAs QDs. Here, the combination of electrochemistry and absorption spectroscopy allows determination of the absolute energy levels of several valence and conduction band states and doping level of native InAs-EDT QDs. Our measurements also give insight into the electronic structure and state-resolved electron conductivity and mobility of InAs QDs. Our measurements are in line with the work of Saha and Guyot-Sionnest that came out during the review of this work. Like them, we find a reversible bleach of the interband transition upon decreasing the voltage and state-resolved conductivity and mobility.[74] The combination of electrochemistry with other in situ spectroscopic techniques can give further insights into this material. For example, the combination of electrochemistry and photoluminescence spectroscopy[40,75] or transient absorption spectroscopy[39] has been used to study charge trapping in other QD materials. Electrochemical doping is also

https://doi.org/10.1021/jacs.5c21128
J. Am. Chem. Soc. 2026, 148, 3938−3943

very promising as a means to access and use intraband transitions for photodetection and light emission in the mid-infrared region as recently demonstrated for InAs QDs.[74]

■ ASSOCIATED CONTENT

Data Availability Statement

The raw and processed data can be found at DOI: 10.5281/zenodo.17662814.

Supporting Information

The Supporting Information is available free of charge at https://pubs.acs.org/doi/10.1021/jacs.5c21128.

Materials and methods, spectroelectrochemical setup, morphological characterization, additional electrochemical characterization of InAs-EDT QDs, and film electron conductivity and mobility (PDF)

■ AUTHOR INFORMATION

Corresponding Authors

Yan B. Vogel − *Institute of Inorganic Chemistry, Department of Chemistry and Applied Biosciences, ETH Zürich, 8093 Zürich, Switzerland; Empa- Swiss Federal Laboratories for Materials Science and Technology, 8600 Dübendorf, Switzerland;* orcid.org/0000-0003-1975-7292; Email: y.b.vogel@tudelft.nl

Maksym V. Kovalenko − *Institute of Inorganic Chemistry, Department of Chemistry and Applied Biosciences, ETH Zürich, 8093 Zürich, Switzerland; Empa- Swiss Federal Laboratories for Materials Science and Technology, 8600 Dübendorf, Switzerland;* orcid.org/0000-0002-6396-8938; Email: mvkovalenko@ethz.ch

Authors

Rui Tao − *Institute of Inorganic Chemistry, Department of Chemistry and Applied Biosciences, ETH Zürich, 8093 Zürich, Switzerland; Empa- Swiss Federal Laboratories for Materials Science and Technology, 8600 Dübendorf, Switzerland*

Hua Chen − *Department of Chemical Engineering, Delft University of Technology, 2629 HZ Delft, The Netherlands;* orcid.org/0009-0002-3391-9403

Lorenzo J.A. Ferraresi − *Institute of Inorganic Chemistry, Department of Chemistry and Applied Biosciences, ETH Zürich, 8093 Zürich, Switzerland; Empa- Swiss Federal Laboratories for Materials Science and Technology, 8600 Dübendorf, Switzerland;* orcid.org/0009-0001-6559-8977

Simon C. Boehme − *Institute of Inorganic Chemistry, Department of Chemistry and Applied Biosciences, ETH Zürich, 8093 Zürich, Switzerland; Empa- Swiss Federal Laboratories for Materials Science and Technology, 8600 Dübendorf, Switzerland;* orcid.org/0000-0002-8399-5773

Dmitry N. Dirin − *Institute of Inorganic Chemistry, Department of Chemistry and Applied Biosciences, ETH Zürich, 8093 Zürich, Switzerland; Empa- Swiss Federal Laboratories for Materials Science and Technology, 8600 Dübendorf, Switzerland;* orcid.org/0000-0002-5187-4555

Ivan Shorubalko − *Empa- Swiss Federal Laboratories for Materials Science and Technology, 8600 Dübendorf, Switzerland;* orcid.org/0000-0001-9868-7303

Arjan J. Houtepen − *Department of Chemical Engineering, Delft University of Technology, 2629 HZ Delft, The Netherlands;* orcid.org/0000-0001-8328-443X

Complete contact information is available at: https://pubs.acs.org/10.1021/jacs.5c21128

Author Contributions

#R.T. and H.C. contributed equally.

Notes

The authors declare no competing financial interest.

■ ACKNOWLEDGMENTS

Y.B.V. acknowledges the support from the Swiss National Science Foundation (222309) and the support provided by Philippe Trüssel (ETH Zürich) for building the PEEK spectroelectrochemical cell and by Carlota Amoros Llonch for taking the TEM image. H.C. thanks the China Scholarship Council for funding (File No. 202206120047). L.J.A.F. acknowledges financial support from Empa (project MetaQD). This publication was created as part of NCCR Catalysis (grant number 225147), a National Centre of Competence in Research funded by the Swiss National Science Foundation. The authors are grateful for access to the Scientific Center for Optical and Electron Microscopy (ScopeM) and its facilities.

■ REFERENCES

(1) Saleem, M. I.; Kyaw, A. K. K.; Hur, J. Infrared Photodetectors: Recent Advances and Challenges toward Innovation for Image Sensing Applications. *Advanced Optical Materials* **2024**, *12*, 2401625.

(2) Vasilopoulou, M.; Fakharuddin, A.; García de Arquer, F. P.; Georgiadou, D. G.; Kim, H.; Mohd Yusoff, A. R. b.; Gao, F.; Nazeeruddin, M. K.; Bolink, H. J.; Sargent, E. H. Advances in Solution-Processed near-Infrared Light-Emitting Diodes. *Nat. Photonics* **2021**, *15*, 656−669.

(3) García de Arquer, F. P.; Talapin, D. V.; Klimov, V. I.; Arakawa, Y.; Bayer, M.; Sargent, E. H. Semiconductor Quantum Dots: Technological Progress and Future Challenges. *Science* **2021**, *373*, No. eaaz8541.

(4) Gong, X.; Yang, Z.; Walters, G.; Comin, R.; Ning, Z.; Beauregard, E.; Adinolfi, V.; Voznyy, O.; Sargent, E. H. Highly Efficient Quantum Dot near-Infrared Light-Emitting Diodes. *Nat. Photonics* **2016**, *10*, 253−257.

(5) Jiang, Y.; Sun, C.; Xu, J.; Li, S.; Cui, M.; Fu, X.; Liu, Y.; Liu, Y.; Wan, H.; Wei, K.; et al. Synthesis-on-Substrate of Quantum Dot Solids. *Nature* **2022**, *612*, 679−684.

(6) Gao, L.; Quan, L. N.; García de Arquer, F. P.; Zhao, Y.; Munir, R.; Proppe, A.; Quintero-Bermudez, R.; Zou, C.; Yang, Z.; Saidaminov, M. I.; et al. Efficient near-Infrared Light-Emitting Diodes Based on Quantum Dots in Layered Perovskite. *Nat. Photonics* **2020**, *14*, 227−233.

(7) Shen, H.; Gao, Q.; Zhang, Y.; Lin, Y.; Lin, Q.; Li, Z.; Chen, L.; Zeng, Z.; Li, X.; Jia, Y.; et al. Visible Quantum Dot Light-Emitting Diodes with Simultaneous High Brightness and Efficiency. *Nat. Photonics* **2019**, *13*, 192−197.

(8) Deng, Y.; Peng, F.; Lu, Y.; Zhu, X.; Jin, W.; Qiu, J.; Dong, J.; Hao, Y.; Di, D.; Gao, Y.; et al. Solution-Processed Green and Blue Quantum-Dot Light-Emitting Diodes with Eliminated Charge Leakage. *Nat. Photonics* **2022**, *16*, 505−511.

(9) Xu, H.; Song, J.; Zhou, P.; Song, Y.; Xu, J.; Shen, H.; Fang, S.; Gao, Y.; Zuo, Z.; Pina, J. M.; et al. Dipole-Dipole-Interaction-Assisted Self-Assembly of Quantum Dots for Highly Efficient Light-Emitting Diodes. *Nat. Photonics* **2024**, *18*, 186−191.

(10) Shirasaki, Y.; Supran, G. J.; Bawendi, M. G.; Bulović, V. Emergence of Colloidal Quantum-Dot Light-Emitting Technologies. *Nat. Photonics* **2013**, *7*, 13−23.

(11) *Restriction of Hazardous Substances in Electrical and Electronic Equipment (Rohs)*. 2021. https://environment.ec.europa.eu/topics/waste-and-recycling/rohs-directive_en (accessed 2025 June).
(12) Hu, C.; Channa, A. I.; Xia, L.; Li, X.; Li, Z.; Wang, Z. M.; Tong, X. Colloidal Inas Quantum Dots: Synthesis, Properties, and Optoelectronic Devices. *Adv. Funct. Mater.* **2025**, *35*, 2500280.
(13) Bahmani Jalali, H.; De Trizio, L.; Manna, L.; Di Stasio, F. Indium Arsenide Quantum Dots: An Alternative to Lead-Based Infrared Emitting Nanomaterials. *Chem. Soc. Rev.* **2022**, *51*, 9861−9881 10.1039/D2CS00490A.
(14) Stavrinadis, A.; Konstantatos, G. Strategies for the Controlled Electronic Doping of Colloidal Quantum Dot Solids. *ChemPhysChem* **2016**, *17*, 632−644.
(15) Wu, P.; Yan, X.-P. Doped Quantum Dots for Chemo/Biosensing and Bioimaging. *Chem. Soc. Rev.* **2013**, *42*, 5489−5521.
(16) Makkar, M.; Viswanatha, R. Frontier Challenges in Doping Quantum Dots: Synthesis and Characterization. *RSC Adv.* **2018**, *8*, 22103−22112.
(17) Mocatta, D.; Cohen, G.; Schattner, J.; Millo, O.; Rabani, E.; Banin, U. Heavily Doped Semiconductor Nanocrystal Quantum Dots. *Science* **2011**, *332*, 77−81.
(18) Norris, D. J.; Efros, A. L.; Erwin, S. C. Doped Nanocrystals. *Science* **2008**, *319*, 1776−1779.
(19) Bryan, J. D.; Gamelin, D. R. Doped Semiconductor Nanocrystals: Synthesis, Characterization, Physical Properties, and Applications. *Progress in Inorganic Chemistry* **2005**, *54*, 47−126.
(20) Asor, L.; Liu, J.; Xiang, S.; Tessler, N.; Frenkel, A. I.; Banin, U. Zn-Doped P-Type Inas Nanocrystal Quantum Dots. *Adv. Mater.* **2023**, *35*, 2208332.
(21) Amit, Y.; Li, Y.; Frenkel, A. I.; Banin, U. From Impurity Doping to Metallic Growth in Diffusion Doping: Properties and Structure of Silver-Doped InAs Nanocrystals. *ACS Nano* **2015**, *9*, 10790−10800.
(22) Asor, L.; Liu, J.; Ossia, Y.; Tripathi, D. C.; Tessler, N.; Frenkel, A. I.; Banin, U. InAs Nanocrystals with Robust P-Type Doping. *Adv. Funct. Mater.* **2021**, *31*, 2007456.
(23) Amit, Y.; Eshet, H.; Faust, A.; Patllola, A.; Rabani, E.; Banin, U.; Frenkel, A. I. Unraveling the Impurity Location and Binding in Heavily Doped Semiconductor Nanocrystals: The Case of Cu in InAs Nanocrystals. *J. Phys. Chem. C* **2013**, *117*, 13688−13696.
(24) Gudjonsdottir, S.; Houtepen, A. J. Permanent Electrochemical Doping of Quantum Dots and Semiconductor Polymers. *Adv. Funct. Mater.* **2020**, *30*, 2004789.
(25) Gudjonsdottir, S.; van der Stam, W.; Koopman, C.; Kwakkenbos, B.; Evers, W. H.; Houtepen, A. J. On the Stability of Permanent Electrochemical Doping of Quantum Dot, Fullerene, and Conductive Polymer Films in Frozen Electrolytes for Use in Semiconductor Devices. *ACS Applied Nano Materials* **2019**, *2*, 4900−4909.
(26) Yu, D.; Wang, C.; Guyot-Sionnest, P. N-Type Conducting CdSe Nanocrystal Solids. *Science* **2003**, *300*, 1277−1280.
(27) Shim, M.; Wang, C.; Norris, D. J.; Guyot-Sionnest, P. Doping and Charging in Colloidal Semiconductor Nanocrystals. *MRS Bull.* **2001**, *26*, 1005−1008 (From Cambridge University Press Cambridge Core).
(28) Vogel, Y. B.; Stam, M.; Mulder, J. T.; Houtepen, A. J. Long-Range Charge Transport Via Redox Ligands in Quantum Dot Assemblies. *ACS Nano* **2022**, *16*, 21216−21224.
(29) Hoyer, P.; Weller, H. Potential-Dependent Electron Injection in Nanoporous Colloidal ZnO Films. *J. Phys. Chem.* **1995**, *99*, 14096−14100.
(30) Roest, A. L.; Houtepen, A. J.; Kelly, J. J.; Vanmaekelbergh, D. Electron-Conducting Quantum-Dot Solids with Ionic Charge Compensation. *Faraday Discuss.* **2004**, *125*, 55−62.
(31) Roest, A. L.; Kelly, J. J.; Vanmaekelbergh, D. Coulomb Blockade of Electron Transport in a ZnO Quantum-Dot Solid. *Applied physics letters* **2003**, *83*, 5530−5532.
(32) Germeau, A.; Roest, A. L.; Vanmaekelbergh, D.; Allan, G.; Delerue, C.; Meulenkamp, E. A. Optical Transitions in Artificial Few-Electron Atoms Strongly Confined inside ZnO Nanocrystals. *Phys. Rev. Lett.* **2003**, *90*, 097401.
(33) Meulenkamp, E. A. Electron Transport in Nanoparticulate ZnO Films. *J. Phys. Chem. B* **1999**, *103*, 7831−7838.
(34) Wehrenberg, B. L.; Guyot-Sionnest, P. Electron and Hole Injection in PbSe Quantum Dot Films. *J. Am. Chem. Soc.* **2003**, *125*, 7806−7807.
(35) Vogel, Y. B.; Pham, L. N.; Stam, M.; Ubbink, R. F.; Coote, M. L.; Houtepen, A. J. Solvation Shifts the Band-Edge Position of Colloidal Quantum Dots by Nearly 1 Ev. *J. Am. Chem. Soc.* **2024**, *146*, 9928−9938.
(36) Engel, J. H.; Surendranath, Y.; Alivisatos, A. P. Controlled Chemical Doping of Semiconductor Nanocrystals Using Redox Buffers. *J. Am. Chem. Soc.* **2012**, *134*, 13200−13203.
(37) Wehrenberg, B. L.; Yu, D.; Ma, J.; Guyot-Sionnest, P. Conduction in Charged PbSe Nanocrystal Films. *J. Phys. Chem. B* **2005**, *109*, 20192−20199.
(38) Shim, M.; Guyot-Sionnest, P. N-Type Colloidal Semiconductor Nanocrystals. *Nature* **2000**, *407*, 981−983.
(39) Boehme, S. C.; Walvis, T. A.; Infante, I.; Grozema, F. C.; Vanmaekelbergh, D.; Siebbeles, L. D. A.; Houtepen, A. J. Electrochemical Control over Photoinduced Electron Transfer and Trapping in CdSe-CdTe Quantum-Dot Solids. *ACS Nano* **2014**, *8*, 7067−7077.
(40) van der Stam, W.; du Fossé, I.; Grimaldi, G.; Monchen, J. O. V.; Kirkwood, N.; Houtepen, A. J. Spectroelectrochemical Signatures of Surface Trap Passivation on CdTe Nanocrystals. *Chem. Mater.* **2018**, *30*, 8052−8061.
(41) Ashokan, A.; Han, J.; Hutchison, J. A.; Mulvaney, P. Spectroelectrochemistry of CdSe/CdxZn1-xS Nanoplatelets. *ACS Nano* **2023**, *17*, 1247−1254.
(42) Ashokan, A.; Hutchison, J. A.; Mulvaney, P. Spectroelectrochemistry of CdSe/CdS Core-Shell Quantum Dots. *Chem. Mater.* **2024**, *36*, 1810−1817.
(43) Ashokan, A.; Mulvaney, P. Spectroelectrochemistry of Colloidal CdSe Quantum Dots. *Chem. Mater.* **2021**, *33*, 1353−1362.
(44) Galland, C.; Ghosh, Y.; Steinbrück, A.; Sykora, M.; Hollingsworth, J. A.; Klimov, V. I.; Htoon, H. Two Types of Luminescence Blinking Revealed by Spectroelectrochemistry of Single Quantum Dots. *Nature* **2011**, *479*, 203−207.
(45) Spittel, D.; Poppe, J.; Meerbach, C.; Ziegler, C.; Hickey, S. G.; Eychmüller, A. Absolute Energy Level Positions in CdSe Nanostructures from Potential-Modulated Absorption Spectroscopy (EMAS). *ACS Nano* **2017**, *11*, 12174−12184.
(46) Liu, H.; Keuleyan, S.; Guyot-Sionnest, P. N- and P-Type HgTe Quantum Dot Films. *J. Phys. Chem. C* **2012**, *116*, 1344−1349.
(47) Chen, M.; Guyot-Sionnest, P. Reversible Electrochemistry of Mercury Chalcogenide Colloidal Quantum Dot Films. *ACS Nano* **2017**, *11*, 4165−4173.
(48) Hudson, M. H.; Chen, M.; Kamysbayev, V.; Janke, E. M.; Lan, X.; Allan, G.; Delerue, C.; Lee, B.; Guyot-Sionnest, P.; Talapin, D. V. Conduction Band Fine Structure in Colloidal HgTe Quantum Dots. *ACS Nano* **2018**, *12*, 9397−9404.
(49) Mulder, J. T.; du Fossé, I.; Alimoradi Jazi, M.; Manna, L.; Houtepen, A. J. Electrochemical P-Doping of CsPbBr3 Perovskite Nanocrystals. *ACS Energy Letters* **2021**, *6*, 2519−2525.
(50) Ding, Z.; Quinn, B. M.; Haram, S. K.; Pell, L. E.; Korgel, B. A.; Bard, A. J. Electrochemistry and Electrogenerated Chemiluminescence from Silicon Nanocrystal Quantum Dots. *Science* **2002**, *296*, 1293−1297.
(51) Fuhr, A. S.; Yun, H. J.; Makarov, N. S.; Li, H.; McDaniel, H.; Klimov, V. I. Light Emission Mechanisms in CuInS2 Quantum Dots Evaluated by Spectral Electrochemistry. *ACS Photonics* **2017**, *4*, 2425−2435.
(52) Pinchetti, V.; Lorenzon, M.; McDaniel, H.; Lorenzi, R.; Meinardi, F.; Klimov, V. I.; Brovelli, S. Spectro-Electrochemical Probing of Intrinsic and Extrinsic Processes in Exciton Recombination in I-III-VI2 Nanocrystals. *Nano Lett.* **2017**, *17*, 4508−4517.
(53) Guyot-Sionnest, P. Charging Colloidal Quantum Dots by Electrochemistry. *Microchimica Acta* **2008**, *160*, 309−314.

https://doi.org/10.1021/jacs.5c21128
J. Am. Chem. Soc. 2026, 148, 3938−3943

(54) Vanmaekelbergh, D.; Houtepen, A. J.; Kelly, J. J. Electrochemical Gating: A Method to Tune and Monitor the (Opto)-Electronic Properties of Functional Materials. *Electrochim. Acta* **2007**, *53*, 1140−1149.
(55) Kim, T.; Park, S.; Jeong, S. Diffusion Dynamics Controlled Colloidal Synthesis of Highly Monodisperse InAs Nanocrystals. *Nat. Commun.* **2021**, *12*, 3013.
(56) Song, J. H.; Choi, H.; Pham, H. T.; Jeong, S. Energy Level Tuned Indium Arsenide Colloidal Quantum Dot Films for Efficient Photovoltaics. *Nat. Commun.* **2018**, *9*, 4267.
(57) Tamang, S.; Lee, S.; Choi, H.; Jeong, S. Tuning Size and Size Distribution of Colloidal InAs Nanocrystals Via Continuous Supply of Prenucleation Clusters on Nanocrystal Seeds. *Chem. Mater.* **2016**, *28*, 8119−8122.
(58) Chen, J.; Zheng, S.; Jia, D.; Liu, W.; Andruszkiewicz, A.; Qin, C.; Yu, M.; Liu, J.; Johansson, E. M. J.; Zhang, X. Regulating Thiol Ligands of P-Type Colloidal Quantum Dots for Efficient Infrared Solar Cells. *ACS Energy Letters* **2021**, *6*, 1970−1979.
(59) Luther, J. M.; Law, M.; Song, Q.; Perkins, C. L.; Beard, M. C.; Nozik, A. J. Structural, Optical, and Electrical Properties of Self-Assembled Films of PbSe Nanocrystals Treated with 1,2-Ethanedithiol. *ACS Nano* **2008**, *2*, 271−280.
(60) Ubbink, R. F.; Vogel, Y. B.; Stam, M.; Chen, H.; Houtepen, A. J. Where Do the Electrons Go? Studying Loss Processes in the Electrochemical Charging of Semiconductor Nanomaterials. *Chem. Mater.* **2025**, *37*, 736−745.
(61) Guyot-Sionnest, P.; Wang, C. Fast Voltammetric and Electrochromic Response of Semiconductor Nanocrystal Thin Films. *J. Phys. Chem. B* **2003**, *107*, 7355−7359.
(62) Banin, U.; Lee, C. J.; Guzelian, A. A.; Kadavanich, A. V.; Alivisatos, A. P.; Jaskolski, W.; Bryant, G. W.; Efros, A. L.; Rosen, M. Size-Dependent Electronic Level Structure of Inas Nanocrystal Quantum Dots: Test of Multiband Effective Mass Theory. *J. Chem. Phys.* **1998**, *109*, 2306−2309.
(63) Banin, U.; Millo, O. Optical and Tunneling Spectroscopy of Semiconductor Nanocrystal Quantum Dots. *Nanocrystal Quantum Dots*; CRC Press: 2017; pp 281−310.
(64) Gudjonsdottir, S.; van der Stam, W.; Kirkwood, N.; Evers, W. H.; Houtepen, A. J. The Role of Dopant Ions on Charge Injection and Transport in Electrochemically Doped Quantum Dot Films. *J. Am. Chem. Soc.* **2018**, *140*, 6582−6590.
(65) Roest, A. L.; Kelly, J. J.; Vanmaekelbergh, D.; Meulenkamp, E. A. Staircase in the Electron Mobility of a ZnO Quantum Dot Assembly Due to Shell Filling. *Phys. Rev. Lett.* **2002**, *89*, 036801.
(66) Alimoradi Jazi, M.; Kulkarni, A.; Sinai, S. B.; Peters, J. L.; Geschiere, E.; Failla, M.; Delerue, C.; Houtepen, A. J.; Siebbeles, L. D. A.; Vanmaekelbergh, D. Room-Temperature Electron Transport in Self-Assembled Sheets of PbSe Nanocrystals with a Honeycomb Nanogeometry. *J. Phys. Chem. C* **2019**, *123*, 14058−14066.
(67) Alimoradi Jazi, M.; Janssen, V. A. E. C.; Evers, W. H.; Tadjine, A.; Delerue, C.; Siebbeles, L. D. A.; van der Zant, H. S. J.; Houtepen, A. J.; Vanmaekelbergh, D. Transport Properties of a Two-Dimensional PbSe Square Superstructure in an Electrolyte-Gated Transistor. *Nano Lett.* **2017**, *17*, 5238−5243.
(68) Yu, D.; Wang, C.; Wehrenberg, B. L.; Guyot-Sionnest, P. Variable Range Hopping Conduction in Semiconductor Nanocrystal Solids. *Phys. Rev. Lett.* **2004**, *92*, 216802.
(69) Yu, D.; Wehrenberg, B. L.; Jha, P.; Ma, J.; Guyot-Sionnest, P. Electronic Transport of N-Type CdSe Quantum Dot Films: Effect of Film Treatment. *Journal of Applied Physics* **2006**, *99*. DOI: 10.1063/1.2192288
(70) Chandler, R.; Houtepen, A.; Nelson, J.; Vanmaekelbergh, D. Electron Transport in Quantum Dot Solids: Monte Carlo Simulations of the Effects of Shell Filling, Coulomb Repulsions, and Site Disorder. *Physical Review B—Condensed Matter and Materials Physics* **2007**, *75*, 085325.
(71) Shin, D.; Jeong, H.; Kim, J.; Jang, E.; Park, Y.; Jeong, S. High Performance Infrared InAs Colloidal Quantum Dot Photodetector with 79% Eqe Enabled by an Extended Absorber Layer. *Advanced Optical Materials* **2025**, *13*, 2401931.
(72) Sun, B.; Najarian, A. M.; Sagar, L. K.; Biondi, M.; Choi, M.-J.; Li, X.; Levina, L.; Baek, S.-W.; Zheng, C.; Lee, S.; et al. Fast near-Infrared Photodetection Using III-V Colloidal Quantum Dots. *Adv. Mater.* **2022**, *34*, 2203039.
(73) Kim, M.; Lee, J.; Jung, J.; Shin, D.; Kim, J.; Cho, E.; Xing, Y.; Jeong, H.; Park, S.; Oh, S. H.; et al. Surface-Originated Weak Confinement in Tetrahedral Indium Arsenide Quantum Dots. *J. Am. Chem. Soc.* **2024**, *146*, 10251−10256.
(74) Saha, S. K.; Guyot-Sionnest, P. Mid-Infrared Intraband Transitions in InAs Colloidal Quantum Dots. **2025**. DOI: 10.48550/arXiv.2512.07600. (accessed 2025-01-14).
(75) van der Stam, W.; Grimaldi, G.; Geuchies, J. J.; Gudjonsdottir, S.; van Uffelen, P. T.; van Overeem, M.; Brynjarsson, B.; Kirkwood, N.; Houtepen, A. J. Electrochemical Modulation of the Photophysics of Surface-Localized Trap States in Core/Shell/(Shell) Quantum Dot Films. *Chem. Mater.* **2019**, *31*, 8484−8493.